Electronic Supplementary Information (ESI) for Analyst.
This journal is © The Royal Society of Chemistry 2023

Electronic Supplementary Information

Quantitative imaging for trace elements in solid samples by online isotope dilution laser ablation-inductively coupled plasma-mass spectrometry

Kayo Yanagisawa,[a] Makoto Matsueda,[a,b] Makoto Furukawa,[a,c] Hiroko Ishiniwa,[d] Toshihiro Wada,[d] Takafumi Hirata [e] and Yoshitaka Takagai*[a,d]

[a] Faculty of Symbiotic Systems Science, Cluster of Science and Technology, Fukushima University, 1 Kanayagawa, Fukushima 960-1296 Japan
[b] Collaborative Laboratories for Advanced Decommissioning Sciences, Sector of Fukushima Research and Development, Japan Atomic Energy Agency, 10-2 Fukasaku, Miharu, Fukushima, 963-7700 Japan
[c] PerkinElmer Japan Co., Ltd., 134 Godo, Hodogaya, Yokohama, Kanagawa, 240-0005 Japan
[d] Institute of Environmental Radioactivity, Fukushima University, 1 Kanayagawa, Fukushima 960-1296, Japan
[e] Geochemical Research Center, Graduate School of Science, The University of Tokyo, 7-3-1 Hongo, Bunkyo-ku, Tokyo, 113-0033 Japan

*To whom correspondence should be addressed: s015@ipc.fukushima-u.ac.jp

Table S1. Operating conditions of the laser ablation and ICP-MS systems (page 1/2)

Laser ablation system	
Model	NWR 213 (Elemental Scientific Lasers)
Laser source	Nd:YAG
Wavelength	213 nm
Ablation time per spot	2 s/shot
Interval time	30 s
Fluence	10 J cm^{-2}
Repetition time	10 Hz
Spot size and shape	20−100 μm; square
Carrier gas and flow rate	0.8 L min^{-1} He
ICP-MS	
Model	NexION 300S (PerkinElmer)
RF power	1600 W
Plasma gas flow rate	18.0 L min^{-1} Ar
Auxiliary gas flow rate	1.2 L min^{-1} Ar
Nebulizer gas flow rate	0.6−0.7 L min^{-1} Ar
Cell gas flow rate	STD mode: non-gas
	DRC mode: 2.6 L min^{-1} CH_4
RPq	STD mode: 0.25
	DRC mode: 0.75
Spray chamber	Original hybrid chamber developed in house
Nebulizers	Concentric nebulizer for liquid port / LA for a gas port
Dwell time per mass	30 ms
Sweep/reading	5
Dead time	35 ns
Measured *m*/*z* (isotopes)	^{44}Ca, ^{54}Fe, ^{56}Fe, ^{57}Fe, and ^{58}Fe (with DRC mode);
	^{84}Sr, ^{86}Sr, ^{87}Sr, and ^{88}Sr (with STD mode)

(Continue to page S3)

Operating conditions of the laser ablation system and ICP-MS (page 2/2)

- The nebulizer gas flow rate was set in the range of 0.6−0.7 L min^{-1}, not exceeding 3% of oxide ratio to singly charged ions ($^{140}Ce^{16}O^{+}/^{140}Ce^{+}$), by measuring 1 μg L^{-1} multi-element standard solution to suppress the production of O-based polyatomic sources of interferences, such as ArO^{+}, CaO^{+} (for Fe analysis[1]), $ArPO^{+}$, and $CaPO^{+}$ (for Sr analysis[2]).
- A dual detector in the ICP-MS was cross-calibrated to optimize the dead time by plotting the pulse count data (maximum counting rate: 2×10^6 cps) against the analog count data (maximum counting rate: 10^8 cps) obtained by measurement with the multi-elements standard solution.
- When the dead time was set to 35 ns, the coefficient of determination (R^2) between the pulse and analog count data exceeded 0.999 in the range of *m*/*z* 7−238.

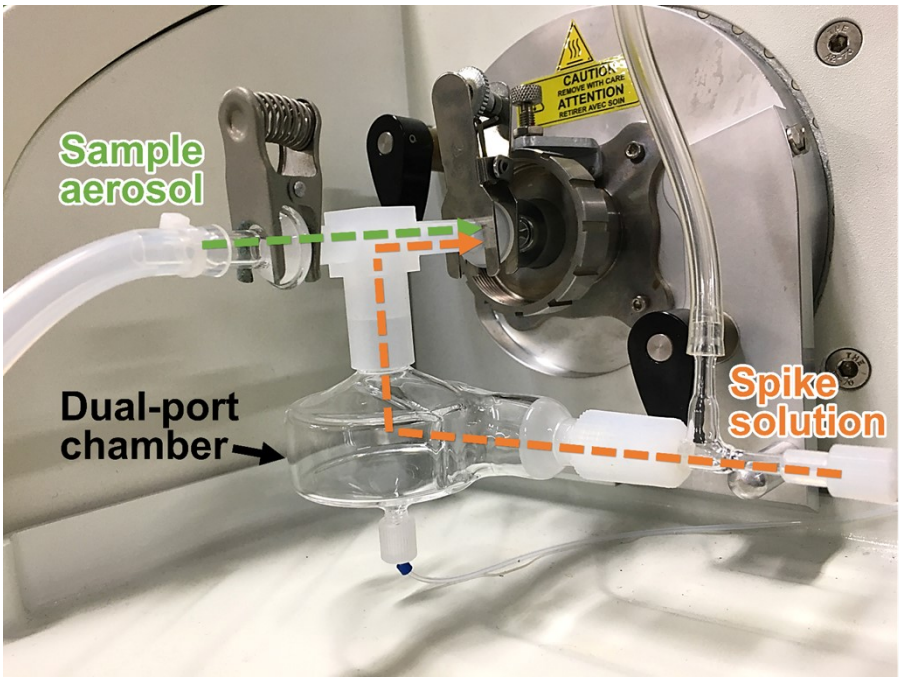

Fig. S1. Photograph of a dual-port chamber.

Fig. S2. Enlarged micrograph (×100) of the Ayu otolith.

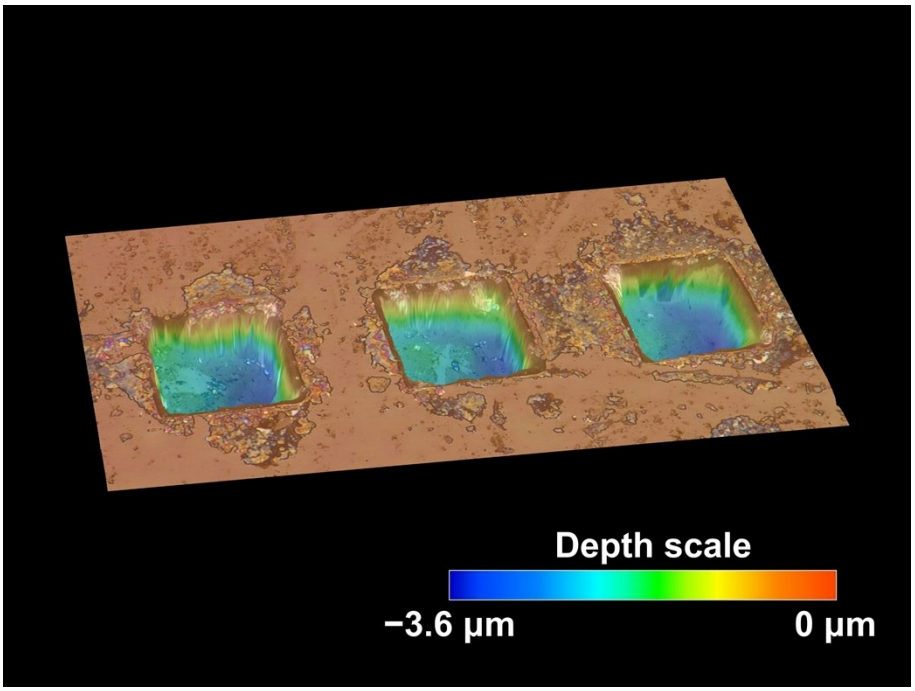

Fig. S3. Example of three-dimensional (3D) shape measurement by using a digital microscope. This photograph shows three craters formed by ablating SRM 610 with a 50 µm square laser shot. The ablated volume (V) is automatically calculated by special software for VHX-8000.

Calculation procedures for transport efficiency in each section (η)

As shown in Figure 1[C] in the text, there are three transport efficiencies (η) for the transport of the ablated particles, mist, or ions from one location to another; i.e., the transport efficiency from the LA to the plasma (η_{LA}), that from the concentric nebulizer to the plasma (η_{CN}), and that from the plasma to the detector (η_I) were calculated using nanoparticles.

Calculation of η: Here, η_{CN} is the mass ratio of the defined amount of the analyte that reaches the plasma through the nebulizer.[3] First, the η_{CN} values were measured using the single-particle mode of the ICP-MS apparatus (sp-ICP-MS) [NexION 300S with a special attachment for single-particle measurements (PerkinElmer Inc.)]. The sp-ICP-MS instrument can count the numbers of nanoparticles as a single pulsed-spike signal, when the dispersed single AuNP is detected. The η_{CN} was determined explained below.

Reagents: A standard solution of monodispersed 49.6 ± 2.1 nm spherical carboxyl polyethylene glycol-coated gold nanoparticles (AuNPs, 9.89×10^6 particle mL^{-1} [equal to 12.4 ng mL^{-1})] dissolved in 1 mM citrate was used [NanoComposix (San Diego, CA, USA)]. The AuNPs (1.0×10^5 particle mL^{-1}) were prepared daily as a working solution with ultrapure water.

Calculations of η: The η_{CN} was calculated using the following equation:

$$\eta_{CN} = \frac{f(I_p)}{q_{liq} t_{dt} C_p} \qquad \text{(Eq. S1)}$$

where $f(I_p)$ is the number of observed pulsed signals per event; q_{liq} is the sample flow rate (mL s^{-1}); t_{dt} is dwell time (s); C_p, is a specific concentration of AuNPs (particle mL^{-1}). Typically, in this study, 1.0×10^5 particle mL^{-1} AuNPs were measured with t_{dt} = 100 s for m/z 197 (as ^{197}Au). The q_{liq} was measured by a TruFlo sample monitor (Glass Expansion, Melbourne, Australia). Data were continuously acquired under the time-resolved analysis mode without any set settling time.

The transmission efficiency from spike solution to the detector (TE_{spk}) is the product of η_{CN} and η_I; the η_I is obtained by dividing TE_{spk} by η_{CN}, as shown in the following Eq. S2. Similar to η_I, η_{LA} is also calculated as the transmission efficiency from the LA system to the detector (TE_{smp}) is divided by η_I, as shown in Eq. S3.

$$\eta_I = \frac{TE_{spk}}{\eta_{CN}} \quad \text{(Eq. S2)}$$

$$\eta_{LA} = \frac{TE_{smp}}{\eta_I} \quad \text{(Eq. S3)}$$

Calculated transmission efficiencies (η_{LA}, η_{CN}, and η_I): These values (η_{LA}, η_{CN}, and η_I) always fluctuate even when measured under certain analytical conditions. However, from the measurements, the η_{LA}, η_{CN}, and η_I were obtained as follows: 2.40×10^{-1}, 7.99×10^{-2}, and 2.04×10^{-5}, respectively [in this measurement, TE_{smp} and TE_{spk} were 4.91×10^{-6} and 1.63×10^{-6}, respectively. Materials: SRM 612 and 1 μg L^{-1} ^{86}Sr-spike were used].

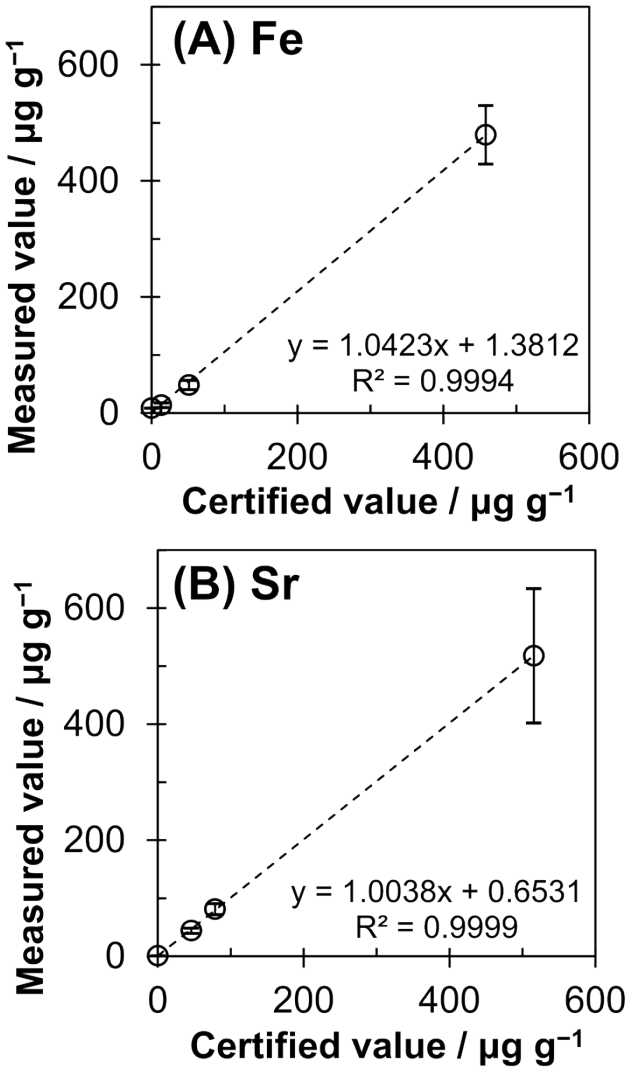

Fig. S4. Linearity between the certified concentrations of the target elements ((A) Fe and (B) Sr) in CRMs and measurement values. Sample: blank (without sample), SRM 610, SRM 612, and SRM 614.

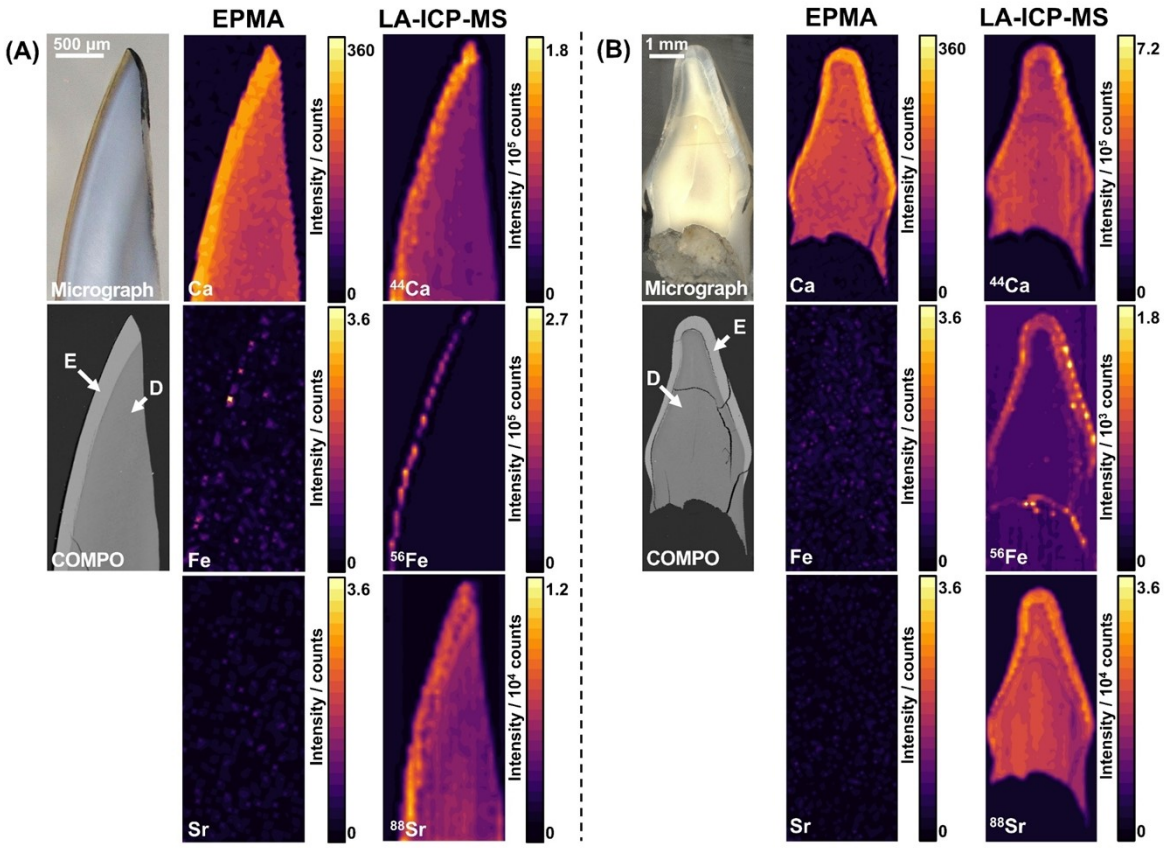

Fig. S5. Elemental imaging of (A) a mouse tooth and (B) a human tooth. Figures on the left show the microscopic image and backscattered electron images. White arrows indicate the enamel (labeled "E") and dentine (labeled "D") layers. The middle figures and figures on the right show the elemental distribution obtained by EPMA (7 μm shot) and LA-ICP-MS (50 μm shot for mouse teeth, 100 μm shot for human teeth).

Prior to the LA-ICP-MS analysis, EPMA analysis was conducted on the samples to evaluate the reliability of the present calibration protocol. The samples coated by Os were analyzed using an electron beam (acceleration voltage: 15 kV, beam current: 10 nA). After EPMA analysis, the samples were polished to form very smoothened surfaces by using abrasive papers (3 μm and 0.05 μm) to analyze it by LA-ICP-MS.

For Ca analysis, the distribution of Ca measured by LA-ICP-MS agreed with the EPMA image. Typically, teeth are mainly composed of $Ca_{10}(PO_4)_6(OH)_2$, and Ca is much more abundant in the enamel than in the dentin. The obtained images reflected this fact. In addition, it is well known that the distribution of Sr in teeth is similar to that of Ca because of their similar chemical properties, though signals for Sr-Lα (1.807 keV) as measured by EPMA were difficult to detect in both types of teeth. Furthermore, Fe analysis in EPMA had relatively poorer sensitivity (Fe-Kα: 6.401 keV) than LA-ICP-MS. Thus, mapping Sr and Fe was difficult, and LA-ICP-MS exhibited better performance in Fe and Sr mapping than EPMA.

References

1 W. M. Thomas and H. W. A. Ray, *At. Spectrosc.*, 1998, **19,** 176–179.

2 M. Willmes, L. Kinsley, M. H. Moncel, R. A. Armstrong, M. Aubert, S. Eggins and R. Grün, *J. Archaeol. Sci.,* 2016, **70**, 102–116.

3 H. E. Pace, N. J. Rogers, C. Jarolimek, V. A. Coleman, C. P. Higgins and J. F. Ranville, *Anal. Chem.*, 2011, **83**, 9361–9369.